DOI: 10.1002/ejic.201000690

Bridged *fac*-Tricarbonylrhenium(I)–Biscarbene Complexes: Synthesis, Characterization, and Molecular Dynamics

Oliver Hiltner,[a] Florian J. Boch,[a] Lennart Brewitz,[a] Peter Härter,[a] Markus Drees,[a] Eberhardt Herdtweck,[a] Wolfgang A. Herrmann,*[a] and Fritz E. Kühn*[a,b]

Keywords: Carbonyl ligands / N ligands / Carbene ligands / Rhenium / Density functional calculations

Six new biscarbene complexes of the type *fac*-[$(CO)_3$-$Re^IBr(L)$], where L represents a chelating bis(N-heterocyclic carbene) ligand consisting of two alkylene-bridged (R′), *N*-substituted (R) imidazoline moieties (1,1′-diR-3,3′-R′-diimidazoline-2,2′-diylidene), were synthesized. Spectroscopic methods and X-ray crystallography were employed to characterize the complexes in solution and the solid state. The observed dynamic behavior of the complexes in solution was examined in more detail by temperature-dependent ^{1}H NMR experiments and further analyzed by DFT calculations.

Introduction

More than forty years ago the first N-heterocyclic carbene complexes were synthesized by means of in situ deprotonation of imidazolium salts with basic metal complexes.[1] In 1991 the first free N-heterocyclic carbene (NHC), 1,3-diadamantylimidazoline-2-ylidene, was isolated sparking a renaissance in the study of these nucleophilic ligands.[2] NHCs were found to be excellent alternatives to phosphane ligands in metal complexes particularly based on their ability to function as strong σ-donor ligands. Organometallic complexes bearing ancillary phosphane ligands have shown a broad range of activity in catalytic applications, and the preparation of NHC analogues has developed into a highly active area of research.[3] Many transition metal complexes containing NHC ligands have been synthesized and were shown to be active homogeneous catalysts, often outperforming their phosphane analogues.[3] It is surprising that only a few rhenium NHC complexes have been synthesized to date, considering the large number of NHC complexes reported, based on other transition metals.

The coordination chemistry of rhenium–NHCs is currently restricted to three formal oxidation states of the metal center. Besides the high-oxidation-state oxo- and nitride-supported $Re^{V/VII}$–NHC complexes,[4,5] the low-valent carbonyl-stabilized Re^I–NHC complexes are the most important representatives. Coordination compounds of the type [$(CO)_{5-n}Re^IXL_n$] (L = imidazolidine-2-ylidene ligands; X = Cl, Br; n = 1, 2) were first examined by Liu et al. and can be obtained by a template-controlled cyclization from an imino-λ^5-phosphane and bromopentacarbonylrhenium(I).[6] Based on this work, Hahn et al. used [$(CO)_4$-Re^IXL] (X = Cl and L = imidazolidine-2-ylidene) to synthesize [$(CO)_3Re^IL'$] (L′ = tridentate macrocycle with two diphenylphosphane substituents bound to the nitrogen atoms of L).[7]

The first rhenium(I) complex containing a chelating bis-NHC ligand, *fac*-[$(CO)_3Re^IIL''$] (L′′ = 1,1′-dimethyl-3,3′-methylenediimidazoline-2,2′-diylidene), was synthesized by Herrmann et al.[8a] by treating $(Me_4N)[Re_2(CO)_6(\mu\text{-}OCH_3)_3]$ with the corresponding imidazolium salt. However, high-pressure conditions were necessary for the synthesis of the metal precursor. In 2008, Perez, Riera and co-workers prepared some new carbonylrhenium(I)–NHC complexes by treating *fac*-tricarbonyltris(*N*-methylimidazole)rhenium(I) with potassium bis(trimethylsilyl)amide.[8b] Recently, we published a new synthetic pathway to generate [$(CO)_3Re^I$-$Br(L'''_2)$] (L′′′ = 1,3-dialkyl-substituted imidazoline-2-ylidene ligand).[8c] Now we are able to extend this synthetic strategy to prepare analogous chelate complexes with bridged bis-NHC ligands. Herein, the preparation of six new air- and moisture-stable complexes of the type *fac*-[$(CO)_3Re^IBr(L)$] where [L = 1,1′-diR-3,3′-R′-diimidazoline-2,2′-diylidene; R′ = CH_2, R = Me (**6a**); R′ = CH_2, R = *i*Pr (**6b**); R′ = C_2H_4, R = Me (**7a**); R′ = C_2H_4, R = *i*Pr (**7b**); R′ = C_2H_4, R = 2,4,6-trimethylphenyl (Mes) (**7c**); R′ = C_2H_4, R = diisopropylphenyl (dipp) (**7d**)] is presented.

Results and Discussion

Synthesis and Characterization of the Rhenium Complexes

The *N*-alkyl- and *N*-aryl-substituted imidazoles were synthesized according to the well-known method of cycliza-

[a] Lehrstuhl für Anorganische Chemie, Catalysis Research Center, Technische Universität München,
Lichtenbergstrasse 4, 85747 Garching, Germany
Fax: +49-89-289-13473
E-mail: fritz.kuehn@ch.tum.de
[b] Molecular Catalysis, Catalysis Research Center, Technische Universität München
Lichtenbergstrasse 4, 85747 Garching, Germany

Supporting information for this article is available on the WWW under http://dx.doi.org/10.1002/ejic.201000690.

tion of glyoxal with ammonium chloride.[9] As shown in Scheme 1, the bridged bis(imidazolium) salts were obtained by S_N2 reactions with dibromomethane and dibromoethane.

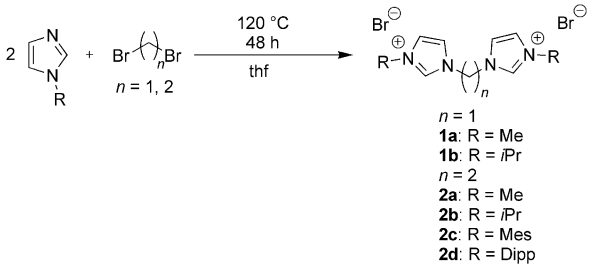

Scheme 1. Synthesis of the bis(imidazolium) bromide salts.

The rhenium precursor $(Et_4N)_2[Re(CO)_3Br_3]$ (**5**) was synthesized at 110 °C by treating $[ReBr(CO)_5]$ with $(Et_4N)Br$ in diglyme.[10]

As illustrated in Scheme 2, the first step in the synthesis of **6a**,**b** and **7a**–**d** was the deprotonation of the imidazolium salts **1a**,**b** and **2a**–**d** with sodium bis(trimethylsilyl)amide (NaBTSA) in thf to generate the free carbenes **3a**,**b** and **4a**–**d** in situ. A thf solution of the free carbenes was then transferred to $(Et_4N)_2[(CO)_3Re^IBr_3]$ (**5**), leading to the formation of **6a**,**b** and **7a**–**d** upon substitution of two of the bromido ligands by one bidentate biscarbene ligand. According to the CO stretching frequencies (see Table 1), the three CO ligands are coordinated to Re^I in a facial fashion with two of the carbonyl ligands occupying the sites *trans* to the NHC units of the chelating biscarbene ligand, whereas the third carbonyl ligand is located *trans* to the bromido ligand. As expected, the CO stretching frequencies for the neutral complexes **6a**,**b** and **7a**–**d** appear at higher wavenumbers than those for the anionic complex **5**.

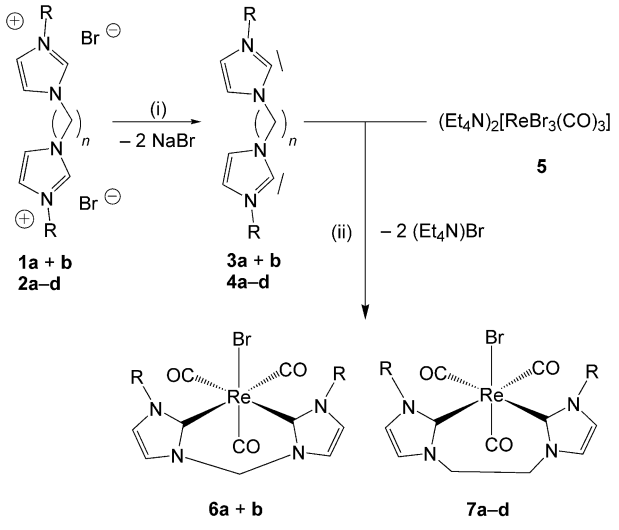

Scheme 2. (i) thf, NaBTSA, n = 1, T = –78 °C, 2 h; n = 2, room temp., 2 h; (ii) thf, room temp., 10 h.

Table 1. The CO stretching frequencies [cm^{-1}] of the rhenium(I) complexes **5**, **6a**,**b**, and **7a**–**d** as a KBr pellet and dissolved in dichloromethane (DCM).

	KBr	DCM
5	1999 vs, 1869 vs	–
6a	2007 s, 1906 vs, 1873 vs	2012 vs, 1918 s, 1873 s
6b	2005 vs, 1894 vs, 1868 vs	2011 vs, 1916 s, 1873 s
7a	2000 vs, 1887 vs, 1859 vs	2009 vs, 1910 s, 1869 s
7b	2006 s, 1901 s, 1853 s	2008 vs, 1910 s, 1868 s
7c	2002 s, 1899 m, 1871 m	2011 vs, 1913 s, 1875 s
7d	2006 s, 1911 m, 1880 m, 1857 m	2008 vs, 1904 s, 1880 s

The ^{13}C NMR spectra of the Re^I–biscarbene complexes support the conclusions drawn from the IR spectra. The observed chemical shifts for selected resonance signals are listed in Table 2. Based on the facial arrangement of the CO ligands, the two resonance signals detected within the range of δ = 191.1 to 196.4 ppm were assigned to the three carbonyl carbon atoms, whereas the peaks found within the range of δ = 171.0 to 176.1 ppm were attributed to the two carbene carbon atoms. As a result of the asymmetric *N*-substitution of the imidazole rings, two peaks for the carbon atoms of the C–C double bond of the imidazole ring were detected ranging from δ = 117.6 to 124.4 ppm.

Table 2. Selected ^{13}C NMR (100 MHz) resonance signals [ppm] of **6a**,**b** and **7a**–**d** in $[D_6]$dmso at room temperature.

Complex	CO^{NHC}	CO^{Br}	NCN (carbene)	NCHCHN
6a	196.4	191.4	174.9	122.6; 121.0
6b	195.9	191.1	173.7	122.0; 117.6
7a	195.0	192.3	171.7	123.7; 122.7
7b	194.3	192.2	171.0	123.6; 118.5
7c	191.6	192.6	175.5	124.4; 122.9
7d (T = 333 K)[a]	191.3	192.2	176.1	123.0; 122.5

[a] The ^{13}C NMR spectrum was recorded at 333 K due to the low solubility of complex **7d** in $[D_6]$dmso.

As expected, the relative chemical shifts of the *trans*-located carbonyl and the NHC carbon atoms (CO^{NHC} and NCN, respectively) differ for the complexes with aryl-substituted NHCs (**7c** and **7d**) and those with alkyl groups as *N*-substituents (**7a** and **7b**), whereas the chemical shifts of the CO carbon atoms *trans* to the bromo ligand (CO^{Br}) are nearly the same. The chemical shifts of the resonance signals detected for **6a**, **6b**, **7a**, and **7b** decrease in the order CO^{NHC} to CO^{Br} to NCN, whereas in case of **7c** and **7d** the order is reversed for CO^{NHC} and CO^{Br}. The resonance signals assigned to the carbene carbon atoms of **7a** and **7b** are observed at higher fields than in the case of **7c** and **7d**. Both observations are consistent with the assumption that the resonance signals appear at lower fields for NCN and at higher fields for CO^{NHC} for the aryl-substituted derivatives compared to their alkyl-substituted analogues, which can be attributed to either the –I effect of the aryl substituents leading to a lower electron density at the metal center or the anisotropy effect of aromatic substituents. In addition, the carbene resonance signals for **7c** and **7d** are shifted to a

lower field than those for **6a** and **6b**. However, the ethylene bridge gives rise to an upfield shift, as seen when comparing **6a** and **6b** with **7a** and **7b**. Accordingly, it appears that the effect of the aryl substituents is comparatively strong.

The analysis of the ^{1}H NMR spectra of the complexes **6a**,**b** and **7a**–**d** reveals differences due to the bridge length of the chelating biscarbene ligand. The following comparison of **6a** and **7a** serves as an example for these general differences. The ^{1}H NMR spectra of the imidazolium salts **1a**,**b** and **2a**–**d** include one singlet that can be assigned to the protons of the methylene and ethylene groups, respectively, indicating the chemical equivalence of the protons. However, upon formation of the biscarbene complexes **6a**,**b** and **7a**–**d** the alkylene protons are no longer equivalent. In the case of **6a**, two doublets for the methylene protons were observed at δ = 5.88 and 6.58 ppm with a coupling constant of ^2J = 13.4 Hz (Figure 1).

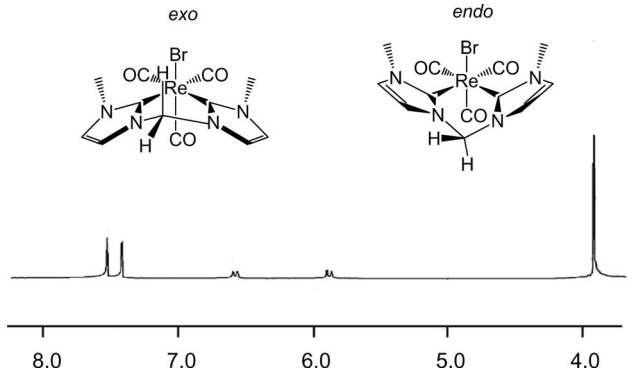

Figure 1. ^{1}H NMR spectrum of **6a** in [D$_6$]dmso, along with the *endo* and the *exo* configuration of the complex.

As for *fac*-[(CO)$_3$Re$^{\mathrm{I}}$IL′′],[8a] this can be attributed to the "flapping-wing"-type motion of the imidazole rings that can result in two possible configurations of the complexes (*endo* or *exo*). Regarding the kinetic NMR studies of **6a** in the following section, it can be concluded that only one configuration exists at room temperature.

The ^{1}H NMR spectrum of **7a** in [D$_6$]dmso, which is depicted in Figure 2, reveals that the ethylene protons have enantiotopic and diastereotopic properties after coordination, and an AA′XX′ spin system describes the observed multiplet at δ = 4.57 and 4.78 ppm with the two coupling constants of ^3J = 8.6 Hz and ^2J = 15.8 Hz. Theoretically, there should be a third coupling constant. However, the two doublets of doublets of doublets cannot be properly resolved by the NMR measurements.

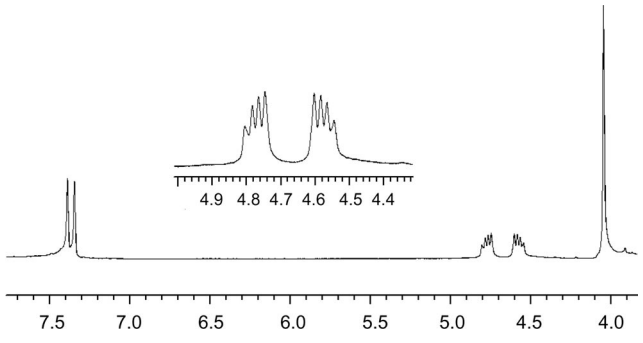

Figure 2. ^{1}H NMR spectrum of complex **7a** in [D$_6$]dmso.

In order to analyze the proposed dynamic behavior of the methylene-bridged complexes, temperature-dependent NMR experiments were performed. The ^{1}H NMR spectra of **6a** determined in [D$_6$]acetone at temperatures ranging from 183 to 313 K are shown in Figure 3.

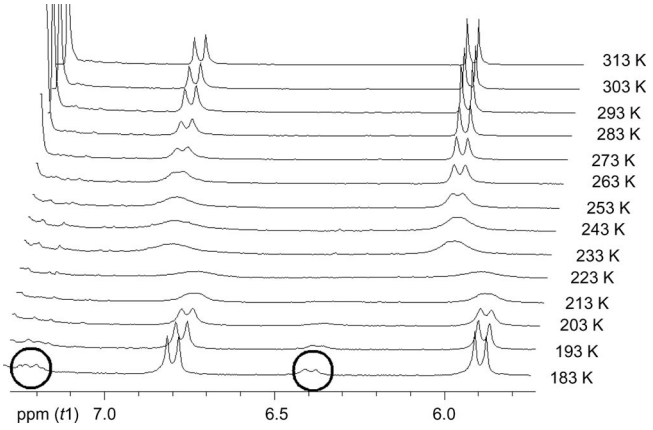

Figure 3. Temperature-dependent ^{1}H NMR spectra of complex **6a** in [D$_6$]acetone.

From the temperature-dependent ^{1}H NMR spectra of complex **6a** it can be seen that there are three temperature intervals during which the characteristics of the signals change significantly. For the interval from 313 to 233 K only one of the two conformers can be observed, indicated by the two doublets at δ = 6.85 and 6.00 ppm. These two doublets smear out at 223 K, which indicates that the coalescence temperature is approximately 220 K ± 1 K. Decreasing the temperature further, the two doublets reappear with a slight change in the chemical shift ($\Delta\delta$ = 0.5–0.1 ppm) to lower values. At 183 K another pair of doublets appear at δ = 7.25 and 6.40 ppm, which belong to the second possible conformer, indicating the coexistence of both states. In summary, it can be assumed that one conformer is kinetically stable only at low temperatures and that a small activation barrier separates both states. In light of this, and because of the previously mentioned small change in the chemical shift of one pair of doublets, only the thermodynamically more stable conformer exists above 193 K.

The ^{1}H NMR spectrum of **6b** in [D$_6$]dmso at room temperature only displays broad resonance signals for the methylene protons and the methyl protons of the isopropyl substituents. Increasing the temperature to 343 K results in a better resolution of all peaks (Figure 4), revealing the two expected doublets for the methylene protons at δ = 5.90 and 6.57 ppm, with a coupling constant of ^2J = 13.2 Hz, and a septet for the methyl protons at δ = 5.28 ppm, with a coupling constant of ^3J = 6.4 Hz.

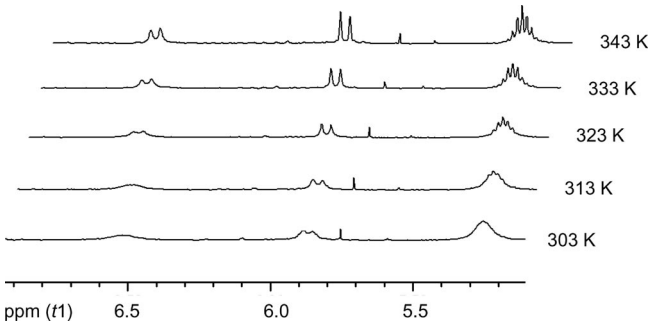

Figure 4. Temperature-dependent ^{1}H NMR spectra of **6b** in [D$_6$]-dmso.

These results indicate coalescence near ambient temperature. To confirm this assumption, temperature-dependent NMR studies of **6b** in [D$_6$]acetone were performed. The series of ^{1}H NMR spectra at different temperatures, which are shown in Figure 5, revealed a coalescence temperature of 283 K. In contrast to **6a**, it was not possible within the chosen temperature range to reach a temperature where the *endo* and *exo* forms coexist.[8a] It was also observed that the doublet at δ = 6.6 ppm does not reappear above 293 K, wheras it is still visible in [D$_6$]dmso. This is possibly the result of a solvent effect.

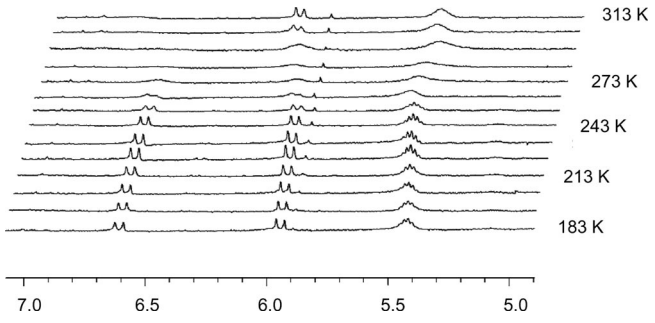

Figure 5. Temperature-dependent ^{1}H NMR spectra of **6b** in [D$_6$]-acetone.

It was not possible to assign the two sets of signals to a specific conformer of **6a**,**b** in solution by standard NMR methods. Therefore the letters A_1 and A_2 were chosen to describe the equilibrium between the conformer conversion shown in Scheme 3.

$$A_1 \underset{k_2}{\overset{k_1}{\rightleftharpoons}} A_2$$

Scheme 3. Equilibrium between the *endo* and the *exo* conformers.

On the basis of the depicted NMR spectra, the rate constants, k, of the described conversion at different temperatures were determined by fitting the spectra using WINDNMR-software.[20] The procedure and the obtained values can be found in the Supporting Information.

The experimentally determined k values were used in an Eyring plot (see Supporting Information) to determine $\Delta H^{\neq}$, the activation enthalpy of the conformer conversion. $\Delta H^{\neq}$ was found to be 6.6 kcal/mol and 10.0 kcal/mol for **6a** and **6b**, respectively.

DFT Study of the *endo*/*exo* Equilibrium Enforced by Conformational Changes in the Alkyl Bridge

In order to explain the conformational change on the basis of the NMR timescale, DFT calculations (B3LYP/6-31G* with Re-ECP) were performed. In this study, the energetic differences between the *exo* and *endo* isomers of the complexes **6a** and **6b** (methylene-bridged) and of the complexes **7a**, **7b**, and **7c** (ethylene-bridged), as well as the corresponding transition states, were investigated. The energy profiles of the conformational flipping of the methylene-bridged complexes in a dmso solution are shown in Figure 6.

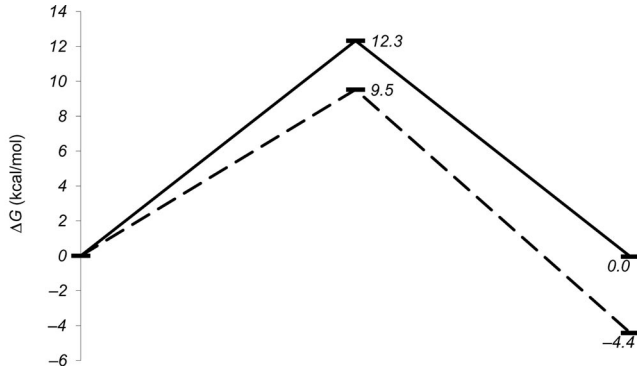

Figure 6. Free-energy plot of the *endo*/*exo* equilibrium for **6a** (solid) and **6b** (dashed) in dmso solution.

In the case of **6a**, which contains an *N*-methyl-substituted biscarbene ligand, the thermodynamic difference between the free energies of the *exo* and the *endo* conformers (see Figure 7 for structures) is 0 kcal/mol. For **6b**, with the biscarbene ligand bearing an *N*-isopropyl substituent, a higher stabilization free energy of 4.4 kcal/mol for the *exo* complex was determined.

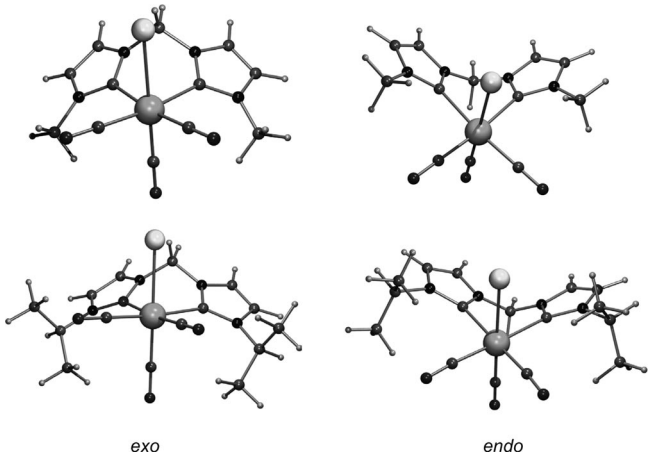

Figure 7. Geometry-optimized structures of the *exo* and *endo* conformers of **6a** (top) and **6b** (bottom).

The transition states for this conformational change have also been calculated for each complex. The results are shown in Figure 8. The free enthalpies of the transition states correspond to the rotational barriers and can be related to the coalescence temperature of the NMR study. In the case of complex **6a**, the barrier $\Delta G^{\neq}$ = 12.3 kcal/mol for both conformers. For **6b**, the activation barrier is 9.5 kcal/mol when starting from the unfavored *endo* conformer and is 13.9 kcal/mol when starting from the favored *exo* conformer. Regarding the ^{1}H NMR spectra of **6a** and **6b** at room temperature, it can be assumed that either only one conformer is preferred at room temperature or that an equilibrium state is detected on the NMR time scale because of the low energy barrier. The two doublets, observed for each methylene-bridged complex dissolved in [D_6]dmso, are evidence for this hypothesis. Due to the higher activation barrier determined for **6b** (starting from the favored *exo* complex), the coalescence temperature should be higher than for **6a**. This is in good agreement with the experimentally estimated rotational barriers where complex **6a** shows coalescence at a lower temperature than **6b** (see NMR studies).

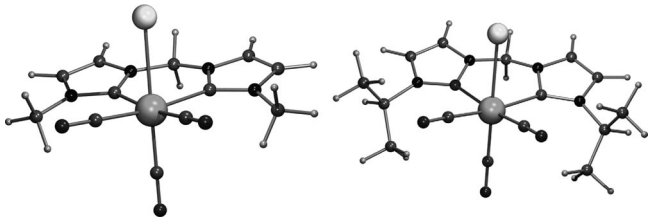

Figure 8. *exo*/*endo* transition states for **6a** (left) and **6b** (right).

The characteristic structural feature of the two transition states is that the NHC rings of the biscarbene ligands, the carbon atom of the methylene bridge, and the two CO ligands are located in the same plane.

DFT calculations considering the *exo* and *endo* conformers, as well as the transition states, of the ethylene-bridged complexes **7a** (*N*-methyl-substituted), **7b** (*N*-isopropyl-substituted), and **7c** (*N*-mesityl-substituted) in the gas phase revealed that for each complex both conformers are energetically identical (see Figure 9). For complex **7c**, which bears the sterically most demanding mesityl substituent, the highest activation barrier was calculated to be 12.2 kcal/mol. For **7a** and **7b**, with smaller *N*-substituents, activation barriers as low as 4.3 and 3.5 kcal/mol, respectively, were obtained. Therefore, complexes **7a** and **7b** should undergo a faster conformational exchange, whereas for **7c** the conformational flipping should occur only at higher temperatures in comparison to the other two complexes.

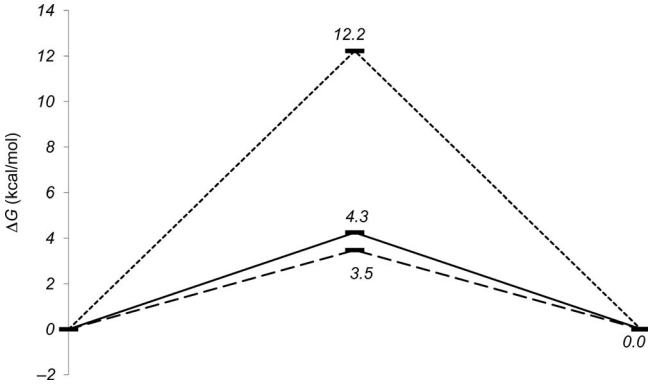

Figure 9. Free-energy plot of the *endo*/*exo* equilibrium for **7a** (solid), **7b** (dashed), and **7c** (dotted).

The characteristic structural feature of the transition states for complexes **7a**–**c** (see Figure 10; R = Mes as an example) for the flipping of the ethylene bridge is that the two carbon atoms are located in such a way that the NHC ends of the bridge are eclipsed. In all the *endo*/*exo* isomers the ethylene bridge atoms assemble more favorably energetically when one of the NHC ends is eclipsed by an H atom of the bridge (see Figure 11; R = Mes as example).

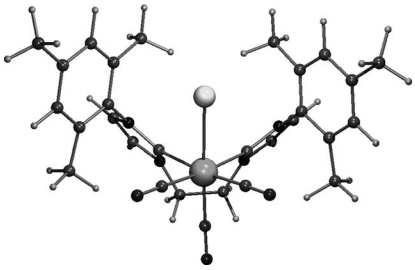

Figure 10. *endo*/*exo* transition state of **7c**.

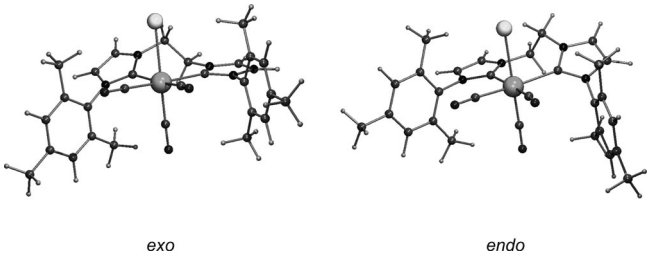

Figure 11. *exo* and *endo* conformations of **7c**; the nomenclature is orientated on the position of the C7 atom of the ethylene bridge with respect to the bromido ligand (for the assignment see the crystallographic section).

Crystallographic Studies

Colorless single crystals of the biscarbene complexes **6a** and **7a**–**c** suitable for the single-crystal X-ray diffraction studies were grown at ambient temperature from a saturated dichloromethane or tetrahydrofurane solution for several days. In agreement with the NMR and IR spectroscopic data, the rhenium atom is coordinated by one bromido, three carbonyl, and one bidentate biscarbene ligand, which forms a slightly distorted octahedron with the bromido and one carbonyl ligand in the apical positions and the two remaining carbonyl ligands in facial positions. Due to a ligand disorder (Br vs. CO) observed in the case of **6a**, only the general crystallographic data are listed in Table 3. Fig-

Table 3. The crystallographic data for compound **6a**·CH_2Cl_2, **7a**·1/2CH_2Cl_2, **7b**, and **7c**.

	6a·CH_2Cl_2[a]	**7a**·1/2CH_2Cl_2
Empirical formula	$C_{12}H_{12}BrN_4O_3Re{\cdot}CH_2Cl_2$	$C_{13}H_{14}BrN_4O_3Re{\cdot}1/2CH_2Cl_2$
Formula mass	611.30	582.86
Color/habit	colorless/fragment	colorless/fragment
Crystal dimensions [mm]		$0.08 \times 0.30 \times 0.38$
Crystal system	monoclinic	monoclinic
Space group	$P2_1/c$ (no. 14)	$P2_1/c$ (no. 14)
a [Å]	7.947(2)	8.3524(3)
b [Å]	14.004(3)	13.8038(6)
c [Å]	14.578(3)	15.0057(6)
α [°]	90	90
β [°]	94.781(12)	95.5902(15)
γ [°]	90	90
V [Å^3]	1616.7(6)	1721.85(12)
Z	4	4
T [K]	123	173
$D_{calcd.}$ [g/cm^3]		2.248
μ [mm^{-1}]		9.552
F (000)		1100
θ range [°]		2.01–25.50
Index ranges (h, k, l)		±8, ±16, ±18
No. of reflections collected		23396
No. of independent reflections/R_{int}		3013/0.036
No. of observed refelections [$I > 2\sigma(I)$]		2868
No. of data/restraints/parameters		3013/0/228
R_1/wR_2 [$I > 2\sigma(I)$][b]		0.0226/0.0592
R_1/wR_2 (all data)[b]		0.0237/0.0605
GOF (on F^2)[b]		1.040
Largest difference peak/hole [e Å^3]		+1.01/–2.45

	7b	**7c**
Empirical formula	$C_{17}H_{22}BrN_4O_3Re$	$C_{29}H_{30}BrN_4O_3Re$
Formula mass	596.50	748.68
Color/habit	colorless/fragment	colorless/fragment
Crystal dimensions [mm]	$0.05 \times 0.08 \times 0.15$	$0.10 \times 0.33 \times 0.53$
Crystal system	triclinic	monoclinic
Space group	$P\bar{1}$ (no. 2)	$P2_1/c$ (no. 14)
a [Å]	8.8081(4)	17.3677(4)
b [Å]	9.2513(4)	10.6016(2)
c [Å]	12.6649(6)	16.4142(3)
α [°]	101.369(2)	90
β [°]	99.492(2)	109.7969(8)
γ [°]	93.233(2)	90
V [Å^3]	993.69(8)	2843.65(10)
Z	2	4
T [K]	173	173
$D_{calcd.}$ [g/cm^3]	1.994	1.749
μ [mm^{-1}]	8.148	5.715
F (000)	572	1464
θ range [°]	6.83–22.21	1.25–25.33
Index ranges (h, k, l)	±9, ±9, ±13	±20, ±12, (–15/19)
No. of reflections collected	9317	88087
No. of independent reflections/R_{int}	2363/0.073	5185/0.032
No. of observed reflections [$I > 2\sigma(I)$]	2240	4975
No. of data/restraints/parameters	2363/0/239	5185/0/349
R_1/wR_2 [$I > 2\sigma(I)$][b]	0.0468/0.1193	0.0146/0.0359
R_1/wR_2 (all data)[b]	0.0481/0.1203	0.0160/0.0374
GOF (on F^2)[b]	1.100	1.078
Largest difference peak/hole [e Å^3]	+3.13/–1.83	+0.87/–0.57

[a] Due to an observed ligand disorder (Br vs. CO), only the basic crystallographic data are given (see Experimental Section). [b] $R_1 = \Sigma(||F_o| - |F_c||)/\Sigma|F_o|$; $wR_2 = \{\Sigma[w(F_o^2 - F_c^2)^2]/\Sigma[w(F_o^2)^2]\}^{1/2}$; GOF = $\{\Sigma[w(F_o^2 - F_c^2)^2]/(n - p)\}^{1/2}$.

ure 12 shows a ball-and-stick representation[11] of **6a** in the solid state, serving as a verification of the basic molecular features. Figures 13, 14, and 15 show ORTEP-style representations of the compounds **7a**–**c**. Selected bond lengths and angles are listed in the figure captions. All bond lengths and bond angles of the N-heterocyclic carbene ligands of the examined compounds lie within the typical ranges. The Re–Br [2.6711(5)–2.6840(3) Å] and Re–C_{CO} bond lengths

[1.902(2)–1.948(2) Å] are within the expected range.[6] The dihedral angles Br1–Re1–C4–N2 of 135.2(3)° (**7a**; R = Me), 137.3(7)° (**7b**; R = *i*Pr), and –88.6(2)° (**7c**; R = Mes), and Br1–Re1–C9–N3/4 of –116.4(3)° (**7a**; R = Me), –117.5(9)° (**7b**; R = *i*Pr), and 49.2(2)° (**7c**; R = Mes) reflect the steric demand of the wing tips (R) and demonstrate the high flexibility of the biscarbene moiety.

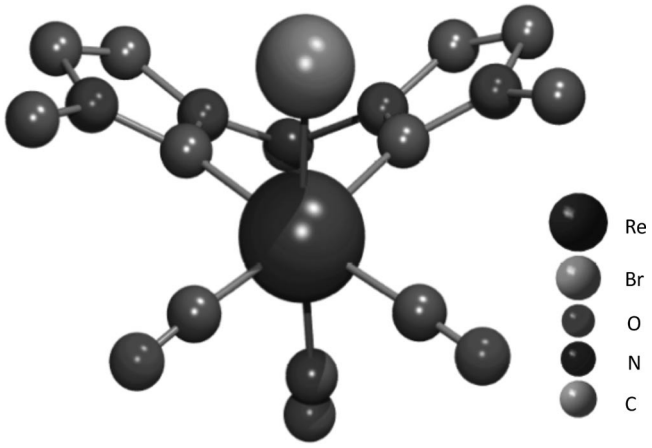

Figure 12. Ball-and-stick representation[11] of **6a**.

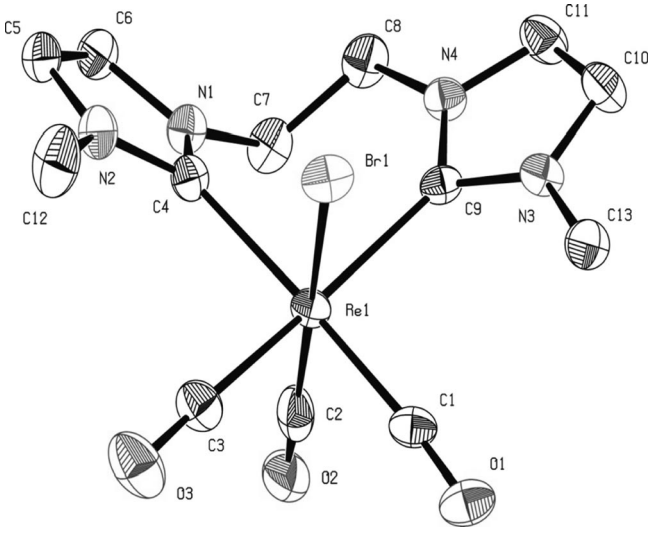

Figure 13. ORTEP-style plot[11] of **7a**; hydrogen atoms are omitted for clarity. Thermal ellipsoids are drawn at the 50% probability level. Selected bond lengths [Å] and bond angles [°]: Re1–Br1 2.6711(5), Re1–C1 1.945(4), Re1–C2 1.931(5), Re1–C3 1.942(4), Re1–C4 2.193(4), Re1–C9 2.236(4), C4–N1 1.346(5), C4–N2 1.368(5), C9–N3 1.368(5), C9–N4 1.375(5); Br1–Re1–C1 89.34(10), Br1–Re1–C2 175.19(14), Br1–Re1–C3 88.18(13), Br1–Re1–C4 90.31(9), Br1–Re1–C9 85.57(9), C1–Re1–C2 87.9(2), C1–Re1–C3 86.4(2), C1–Re1–C4 177.4(2), C1–Re1–C9 93.1(2), C2–Re1–C3 87.8(2), C2–Re1–C4 92.3(2), C2–Re1–C9 98.5(2), C3–Re1–C4 91.0(2), C3–Re1–C9 173.7(2), C4–Re1–C9 89.4(2), N1–C4–N2 103.2(3), N3–C9–N4 102.4(3).

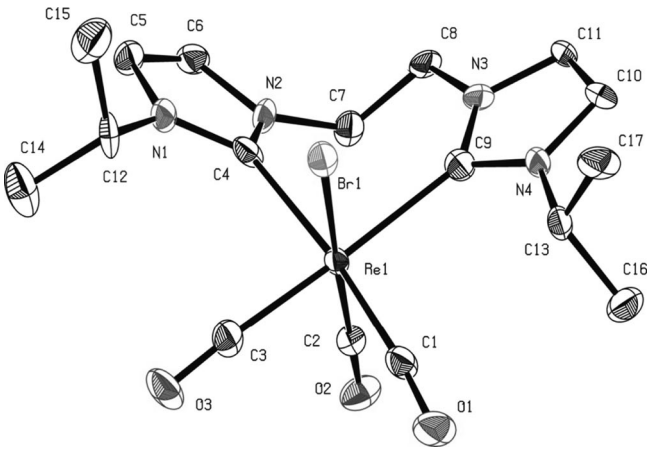

Figure 14. ORTEP-style plot[11] of **7b**; hydrogen atoms are omitted for clarity. Thermal ellipsoids are drawn at the 50% probability level. Selected bond lengths [Å] and bond angles [°] are: Re1–Br1 2.6721(10), Re1–C1 1.929(11), Re1–C2 1.933(10), Re1–C3 1.935(10), Re1–C4 2.208(10), Re1–C9 2.248(9), C4–N1 1.357(12), C4–N2 1.369(11), C9–N3 1.374(11), C9–N4 1.372(11); Br1–Re1–C1 89.9(3), Br1–Re1–C2 176.4(3), Br1–Re1–C3 94.0(3), Br1–Re1–C4 89.5(2), Br1–Re1–C9 83.8(2), C1–Re1–C2 86.5(4), C1–Re1–C3 85.2(4), C1–Re1–C4 173.6(3), C1–Re1–C9 96.3(3), C2–Re1–C3 85.9(4), C2–Re1–C4 94.2(4), C2–Re1–C9 96.5(3), C3–Re1–C4 88.5(4), C3–Re1–C9 177.3(4), C4–Re1–C9 90.0(3), N1–C4–N2 104.0(8), N3–C9–N4 102.8(7).

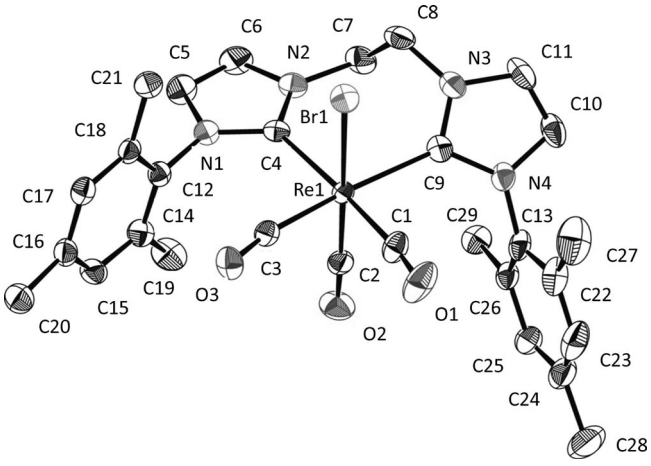

Figure 15. ORTEP-style plot[11] of compound **7c**; hydrogen atoms are omitted for clarity. Thermal ellipsoids are drawn at the 50% probability level. Selected bond lengths [Å] and bond angles [°] are: Re1–Br1 2.6840(3), Re1–C1 1.943(3), Re1–C2 1.902(2), Re1–C3 1.948(2), Re1–C4 2.226(2), Re1–C9 2.212(2), C4–N1 1.369(3), C4–N2 1.366(3), C9–N3 1.357(3), C9–N4 1.370(3); Br1–Re1–C1 88.49(9), Br1–Re1–C2 177.11(7), Br1–Re1–C3 89.08(7), Br1–Re1–C4 90.07(6), Br1–Re1–C9 85.49(6), C1–Re1–C2 89.56(11), C1–Re1–C3 81.62(11), C1–Re1–C4 175.82(10), C1–Re1–C9 89.15(11), C2–Re1–C3 88.53(10), C2–Re1–C4 91.73(9), C2–Re1–C9 96.61(9), C3–Re1–C4 94.43(9), C3–Re1–C9 169.41(9), C4–Re1–C9 94.66(8), N1–C4–N2 102.1(2), N3–C9–N4 103.2(2).

Conclusions

Six biscarbene complexes of the type *fac*-[$(CO)_3Re^{I}Br$-(L)], with the bis-NHC ligands (L) differing in the bridge

length (methylene and ethylene) and the *N*-substituents (Me, *i*Pr, Mes, and dipp), were obtained by treating the in situ generated free biscarbenes with *fac*-[$(CO)_3Re^IBr_3$]. All six compounds were thoroughly analyzed by spectroscopic methods, and crystal structures were determined for four of the complexes. Based on the CO stretching frequencies obtained from the different *N*-alkyl substitutents, it can be concluded that these *N*-alkyl subsituents have a very limited effect on the electron density of the rhenium center. On the contrary, the bridging group significantly influences the σ-donor property of the corresponding biscarbene. The chemical shifts of the ^{13}C NMR signals, attributed to the carbonyl and carbene carbon atoms, differ significantly only for complexes containing different *N*-alkyl bridges. Kinetic NMR studies revealed that the chelating ligands of **6a** and **6b** undergo a flipping motion in solution by rotating their imidazole rings. The experimentally determined energy barriers for this conversion were confirmed by applying DFT methods to calculate the free energies for the geometry-optimized conformers and the transition state. Due to the high stability of the complexes in air and water, some of the synthesized complexes could be used as radiopharmaceuticals, by replacing the rhenium by its radioactive isotopes or the homologous technetium.

Experimental Section

General: All preparations were carried out under argon by using standard Schlenk techniques. Solvents were dried and degassed according to standard methods prior to use. All *N*-alkyl- and *N*-aryl-substituted imidazoles were synthesized by the well-known cyclization of glyoxal and ammonium chloride.[9] The bridged bis(imidazolium) salts, **1a**,**b** and **2a**–**d**, were obtained by S_N2 reactions of the imidazoles with dibromomethane and dibromoethane, respectively. Compound **5** was prepared by treating [$ReBr(CO)_5$] and $(Et_4N)Br$ in diglyme at 110 °C as previously described.[10] All other chemicals were purchased from commercial vendors and used as received. NMR spectra were recorded with a Jeol JNM GX400 and a Bruker Avance DPX 400 NMR spectrometers. IR spectra were measured with a Jasco FTIR 460plus spectrometer. Electronic and chemical ionization mass spectra were obtained with a Finnigan MAT90 spectrometer. Elemental analyses were performed in the Microanalytical Laboratory of the Department of Chemistry at the Technische Universitaet München.

***fac*-Bromotricarbonyl(1,1′-dimethyl-3,3′-methylenediimidazoline-2,2′-diylidene)rhenium(I) (6a):** A solution of sodium bis(trimethylsilyl)amide (0.52 mmol) in thf (2 M) was added dropwise by syringe to **1a** (0.088 g, 0.26 mmol) suspended in thf (15 mL) at –78 °C. The yellow reaction mixture was stirred for 2 h to obtain a colorless solution containing the free carbene **3a** before it was transferred to a Schlenk tube containing **5** (0.2 g, 0.26 mmol). After stirring at ambient temperature for 10 h, the resulting suspension was filtered through a short silica gel column. The solvent was removed from the dark yellow filtrate under reduced pressure to obtain a yellow solid, which was washed with *n*-hexane (2 × 2 mL), diethyl ether (2 × 2 mL), and ethanol (2 × 1.5 mL) at –78 °C. The colorless product **6a** was then dried in vacuo overnight; **6a** is soluble in thf, dichloromethane, and stable upon exposure to air and moisture. Yield: 0.034 g (0.065 mmol, 25%). IR (KBr): $\tilde{\nu}$ = 2007 (s, CO), 1906 (vs, CO), 1873 (vs, CO) cm^{-1}. IR (DCM): $\tilde{\nu}$ = 2012 (vs, CO), 1918 (s, CO), 1873 (s, CO) cm^{-1}. ^1H NMR (400 MHz, [D_6]dmso, 298 K): δ = 3.92 (s, 6 H, NCH_3), 5.88 (d, ^2J = 13.4 Hz, 1 H, NC*H*HN), 6.58 (d, ^2J = 13.4 Hz, 1 H, NCH*H*N), 7.42 (d, ^2J = 1.0 Hz, 2 H, NC*H*CHN), 7.53 (d, ^2J = 1.0 Hz, 2 H, NCHC*H*N) ppm. ^{13}C NMR (100.5 MHz, [D_6]dmso, 298 K): δ = 38.2 (N*C*H_3),62.8 (N*C*H_2N), 121.0 (N*C*HCHN), 122.6 (NCH*C*HN), 174.9 (N*C*N), 191.4 ($CO_{cis\text{-}NHC}$), 196.4 ($CO_{trans\text{-}NHC}$) ppm. $C_{12}H_{12}BrN_4O_3Re$·0.5thf (554.42): calcd. C 29.90, H 2.87, N 9.96; found C 30.33, H 3.20, N 9.67.

***fac*-Bromotricarbonyl(1,1′-diisopropyl-3,3′-methylenediimidazoline-2,2′-diylidene)rhenium(I) (6b):** Compound **6b** was prepared analogously to **6a**. Yield: 0.056 g (0.096 mmol, 37%). IR (KBr): $\tilde{\nu}$ = 2005 (vs, CO), 1894 (vs, CO), 1868 (s, CO) cm^{-1}. IR (DCM): $\tilde{\nu}$ = 2011 (vs, CO), 1916 (s, CO), 1873 (s, CO) cm^{-1}. ^1H NMR (400 MHz, [D_6]dmso, 298 K): δ = 1.42 [d, ^3J = 6.8 Hz, 12 H, NCH(CH_3)$_2$], 5.25 [m, 2 H, NC*H*(CH_3)$_2$], 5.86 (m, 2 H, NC*H*HN), 6.51 (m, 2 H, NCH*H*N), 7.58 (s, 2 H, NC*H*CHN), 7.60 (s, 2 H, NCHC*H*N) ppm. ^1H NMR (400 MHz, [D_6]dmso, 343 K): δ = 1.43 [d, ^3J = 6.4 Hz, 12 H, NCH(CH_3)$_2$], 5.28 [m, ^3J = 6.4 Hz, 2 H, NC*H*(CH_3)$_2$], 5.9 (d, ^2J = 13.2 Hz, 2 H, NC*H*HN), 6.57 (d, ^2J = 13.2 Hz, 2 H, NCH*H*N), 7.55 (s, 2 H, NC*H*CHN), 7.56 (s, 2 H, NCHC*H*N) ppm. ^{13}C NMR (100.5 MHz, [D_6]dmso, 298 K): δ = 22.7 [NCH(*C*H_3)$_2$], 23.4 [NCH(*C*H_3)$_2$], 52.2 [N*C*H(CH_3)$_2$], 62.8 (N*C*H_2N), 117.6 (N*C*HCHN), 122.0 (NCH*C*HN), 173.7 (N*C*N), 191.1 ($CO_{cis\text{-}NHC}$), 195.9 ($CO_{trans\text{-}NHC}$) ppm. CI-MS: *m*/*z* (%) = 582.5 (48) $[M]^+$, 553.5 (6) $[M - H - CO]^+$, 502.6 (100) $[M - Br]^+$. $C_{16}H_{20}BrN_4O_3Re$ (582.47): calcd. C 32.99, H 3.46, N 9.62; found C 33.64, H 3.54, N 9.89.

***fac*-Bromotricarbonyl(1,1′-dimethyl-3,3′-ethylenediimidazoline-2,2′-diylidene)rhenium(I) (7a):** Compound **7a** was prepared analogously to **6a**. Yield: 0.078 g (0.143 mmol, 55%). IR (KBr): $\tilde{\nu}$ = 2000 (vs, CO), 1887 (vs, CO), 1859 (vs, CO) cm^{-1}. IR (DCM): $\tilde{\nu}$ = 2009 (vs, CO), 1910 (s, CO), 1868 (s, CO) cm^{-1}. ^1H NMR (400 MHz, [D_6]dmso, 298 K): δ = 4.05 (s, 6 H, NCH_3); 4.57 (ddd, ^3J = 8.6 Hz, ^2J = 15.8 Hz, 2 H, NC*H*HC*H*HN), 4.78 (ddd, ^3J = 8.6 Hz, ^2J = 15.8 Hz, 2 H, NCH*H*CH*H*N), 7.35 (d, ^3J = 1.6 Hz, 2 H, NC*H*CHN), 7.39 (d, ^3J = 1.6 Hz 2 H, NCHC*H*N) ppm. ^{13}C NMR (100.5 MHz, [D_6]dmso, 298 K): δ = 40.0 (N*C*H_3),49.5 (N*C*H_2*C*H_2N), 122.7 (N*C*HCHN), 123.7 (NCH*C*HN), 171.7 (N*C*N), 192.3 ($CO_{cis\text{-}NHC}$), 195.0 ($CO_{trans\text{-}NHC}$) ppm. CI-MS: *m*/*z* (%) = 539.6 $[M - H]^+$, (16.2), 485.5 (39.5) $[M - H - 2\ CO]^+$, 460.7 (100) $[M - Br]^+$. $C_{13}H_{14}BrN_4O_3Re$ (540.39): calcd. C 28.89, H 2.61, N 10.37; found C 29.21, H 2.97, N 10.26.

***fac*-Bromotricarbonyl(1,1′-diisopropyl-3,3′-ethylenediimidazoline-2,2′-diylidene)rhenium(I) (7b):** Compound **7b** was prepared analogously to **6a**. Yield: 0.091 g (0.152 mmol, 59%). IR (KBr): $\tilde{\nu}$ = 2006 (s, CO), 1901 (s, CO), 1853 (s, CO) cm^{-1}. IR (DCM): $\tilde{\nu}$ = 2008 (vs, CO), 1910 (s, CO), 1868 (s, CO) cm^{-1}. ^1H NMR (400 MHz, [D_6]dmso, 298 K): δ = 1.38 [dd, ^3J = 6.4 Hz, 12 H, NCH(CH_3)$_2$], 4.51 (ddd, ^3J = 8.8 Hz, ^2J = 14.8 Hz, 2 H, NC*H*HC*H*HN), 4.87 (ddd, ^3J = 8.8 Hz, ^2J = 14.8 Hz, 2 H, NCH*H*CH*H*N), 5.65 [sept, ^3J = 6.4 Hz, 2 H, NC*H*(CH_3)$_2$], 7.58 (d, ^3J = 1.8 Hz, 2 H, NC*H*CHN), 7.39 (d, ^3J = 1.8 Hz, 2 H, NCHC*H*N) ppm. ^{13}C NMR (100.5 MHz, [D_6]dmso, 298 K): δ = 23.4 [NCH(*C*H_3)$_2$], 23.7 [NCH(*C*H_3)$_2$], 49.3 (N*C*H_2*C*H_2N), 52.7 [N*C*H(CH_3)$_2$], 118.5 (N*C*HCHN), 123.6 (NCH*C*HN), 171.0 (N*C*N), 192.2 ($CO_{cis\text{-}NHC}$), 194.3 ($CO_{trans\text{-}NHC}$) ppm. CI-MS: *m*/*z* (%) = 595.6 (15.9) $[M - H]^+$, 541.7 (13) $[M + H - 2\ CO]^+$, 516.6 (100) $[M - Br]^+$. $C_{17}H_{22}BrN_4O_3Re$ (596.49): calcd. C 34.23, H 3.72, N 9.39; found C 34.49, H 3.61, N 9.14.

***fac*-Bromotricarbonyl[1,1′-(2′′,4′′,6′′-trimethylphenyl)-3,3′-ethylenediimidazoline-2,2′-diylidene]rhenium(I) (7c):** Compound **7c** was

prepared analogously to **6a**. Yield: 0.074 g (0.099 mmol, 38%). IR (KBr): $\tilde{\nu}$ = 2002 (s, CO), 1899 (m, CO), 1871 (m, CO) cm^{-1}. IR (DCM): $\tilde{\nu}$ = 2011 (vs, CO), 1913 (s, CO), 1871 (s, CO) cm^{-1}. ^1H NMR (400 MHz, [D$_6$]dmso, 298 K): δ = 1.90 (s, 6 H, *ortho*-CH_3), 2.02 (s, 6 H, *ortho*-CH_3), 2.25 (s, 6 H, *para*-CH_3), 4.33 (ddd, ^3J = 7.1 Hz, ^2J = 14.2 Hz, 2 H, NCH*H*CH*H*N), 5.28 (ddd, ^3J = 7.2 Hz, ^2J = 14.3 Hz, 2 H, NC*H*HC*H*HN), 6.95 (s, 4 H, *meta*-C*H*), 7.19 (s, 2 H, NC*H*CHN), 7.56 (s, 2 H, NCHC*H*N) ppm. ^{13}C NMR (100.5 MHz, [D$_6$]dmso, 298 K): δ = 17.78 (*ortho*-*C*H$_3$), 18.36 (*ortho*-*C*H$_3$), 20.66 (*para*-*C*H$_3$), 40.43 (N*C*H$_2$CH$_2$N), 51.55 (NCH$_2$*C*H$_2$N), 122.88 (N*C*HCHN), 124.39 (NCH*C*HN), 128.52 [*para*-*C*(CH$_3$)], 128.77 (*meta*-*C*H), 135.5 [*ortho*-*C*(CH$_3$)], 136.32 [*ortho*-*C*(CH$_3$)], 137.8 (*ipso*-*C*N), 138.26 (*ipso*-*C*N), 175.45 (N*C*N), 191.61 (*C*O$_{trans\text{-}NHC}$), 192.63 (*C*O$_{cis\text{-}NHC}$) ppm. $C_{29}H_{30}BrN_4O_3Re$ (748.68): calcd. C 46.52, H 4.04, N 7.48; found C 46.76, H 4.15, N 7.36.

***fac*-Bromotricarbonyl[1,1′-(2′′,6′′-diisopropylphenyl)-3,3′-ethylenediimidazoline-2,2′-diylidene]rhenium(I) (7d):** Compound **7d** was prepared analogously to **6a**. Yield: 0.063 g (0.075 mmol, 29%). IR (KBr): $\tilde{\nu}$ = 2006 (s, CO), 1911 (m, CO), 1880 (m, CO), 1857 (m, CO) cm^{-1}. IR (DCM): $\tilde{\nu}$ = 2008 (vs, CO), 1904 (s, CO), 1880 (s, CO) cm^{-1}. ^1H NMR (400 MHz, [D$_6$]dmso, 298 K): δ = 0.98 [t, ^3J = 6.4 Hz, 12 H, CH(CH_3)$_2$], 1.15 [t, ^3J = 5.5 Hz, 12 H, CH-(CH_3)$_2$], 2.59 [m, 2 H, C*H*(CH$_3$)$_2$], 2.67 [m, 2 H, C*H*(CH$_3$)$_2$], 4.47 (m, 2 H, NCH$_2$CH_2N), 4.92 (ddd, ^3J = 6.8 Hz, ^2J = 14.7 Hz, 2 H, NCH_2CH$_2$N), 7.23 (d, ^3J = 7.7 Hz, 4 H, *meta*-C*H*), 7.34 (s, 2 H, NC*H*CHN), 7.39 (virt. t, ^3J = 7.7 Hz, 2 H, *para*-C*H*), 7.56 (s, 2 H, NCHC*H*N) ppm. ^{13}C NMR (100.5 MHz, [D$_6$]dmso, 333 K): δ = 21.94 [CH(*C*H$_3$)$_2$], 22.73 [CH(*C*H$_3$)$_2$], 25.48 [CH(*C*H$_3$)$_2$], 25.55 [CH(*C*H$_3$)$_2$], 27.2 [*C*H(CH$_3$)$_2$], 27.76 [*C*H(CH$_3$)$_2$], 51.97 (N*C*H$_2$*C*H$_2$N), 122.51 (N*C*HCHN), 123.02 (NCH*C*HN), 123.79 (*para*-*C*), 125.0 (*meta*-*C*), 129.79 (*ortho*-*C*), 137.71 (*ortho*-*C*), 145.63 (*ipso*-*C*N), 146.84 (*ipso*-*C*N), 176.11 (N*C*N), 191.3 (*C*O$_{trans\text{-}NHC}$), 192.19 (*C*O$_{cis\text{-}NHC}$) ppm. $C_{35}H_{42}BrN_4O_3Re$ (832.84): calcd. C 50.47, H 5.08, N 6.73; found C 50.77, H 4.98, N 6.46.

Single-Crystal X-ray Structure Determination of Compounds 6a·CH$_2$Cl$_2$, 7a·1/2CH$_2$Cl$_2$, 7b, and 7c. General: The crystal data and the details of the structure determination are presented in Table 3. Preliminary examination and data collection were carried out with an area detecting system (APEX II, κ-CCD) by using graphite-monochromated Mo-K_α radiation (λ = 0.71073 Å) from a Bruker AXS FR591 generator with a rotating anode. Raw data were corrected for Lorentz, polarization, and, arising from the scaling procedure, for latent decay and absorption effects. The structures were solved by a combination of direct methods and difference Fourier syntheses. All non-hydrogen atoms were refined with anisotropic displacement parameters. Methyl hydrogen atoms were refined as part of rigid rotating groups, with d(C–H) = 0.98 Å and $U_{iso(H)}$ = 1.5$U_{eq(C)}$. All other hydrogen atoms were placed in calculated positions and refined by using a riding model, with methyne, methylene and aromatic C–H distances of 1.00, 0.99, and 0.95 Å, respectively, and $U_{iso(H)}$ = 1.2$U_{eq(C)}$. Full-matrix least-squares refinements were carried out by minimizing $\Sigma w(F_o^2 - F_c^2)^2$ with the SHELXL-97 weighting scheme.[11] The final residual electron density maps showed no remarkable features. Neutral atom scattering factors for all atoms and anomalous dispersion corrections for the non-hydrogen atoms were taken from the International Tables for Crystallography.[11] **Complex 6a**: Data collection was performed at 123 K (Oxford Cryosystems). In an early stage of the refinement routine an unresolvable disorder of the bromido ligand and a carbonyl group was established. Due to this fact, and the incomplete model, the refinements were aborted. However, the basic molecular features were verified. **Complex 7a**: Data collection was performed at 173 K (Oxford Cryosystems) within a θ range of 2.01° < θ < 25.50°. Five data sets were measured in the rotation-scan mode with $\Delta\phi/\Delta\Omega$ = 0.50°. A total number of 23396 intensities were integrated and scaled. After merging (R_{int} = 0.036), a sum of 3013 (all data) and 2868 [$I > 2\sigma(I)$], respectively, remained, and all the data were used. In addition one half solvent molecule CH_2Cl_2 was found in the asymmetric unit cell arranged around a center of symmetry. **Complex 7b**: Data collection was performed at 173 K (Oxford Cryosystems) within a θ range of 2.63° < θ < 25.44°. Three data sets were measured in the rotation-scan mode with $\Delta\phi/\Delta\Omega$ = 0.50°. A total number of 12098 intensities were integrated and scaled. The results of the refinements suffered from the use of a very small and low-quality crystal. As a consequence, the data had to be reduced to a resolution limit in between 6.83° < θ < 22.21°. After merging the 9317 remaining intensities (R_{int} = 0.073), a sum of 2363 (all data) and 2240 [$I > 2\sigma(I)$], respectively, remained, and all the data were used. **Complex 7c**: Data collection was performed at 173 K (Oxford Cryosystems) within a θ range of 1.25° < θ < 25.33°. Nine data sets were measured in the rotation-scan mode with $\Delta\phi/\Delta\Omega$ = 0.50°. A total number of 88087 intensities were integrated and scaled. After merging (R_{int} = 0.032), a sum of 5185 (all data) and 4975 [$I > 2\sigma(I)$], respectively, remained, and all the data were used. Crystallographic data (excluding structure factors) for the structures reported in this paper have been deposited with the Cambridge Crystallographic Data Centre. CCDC-782967 (**7a**·1/2CH$_2$Cl), -782968 (**7b**), and -782969 (**7c**) contain the supplementary crystallographic data for this paper. These data can be obtained free of charge from The Cambridge Crystallographic Data Centre via www.ccdc.cam.ac.uk/data_request/cif.

Computational Details: All the calculations were performed with GAUSSIAN 03[12] by using the density functional/Hartree–Fock hybrid model Becke3LYP[13] and the split-valence double-ζ (DZ) basis set 6-31G*.[14] The Re atoms were described with a Hay–Wadt ECP,[15] with a DZ description of the valence electrons. No symmetry or internal coordinate constraints were applied during the optimizations. All reported intermediates were verified as being true minima by the absence of negative eigenvalues in the vibrational frequency analysis, whereas transition states were located according to the Berny algorithm. Transition state structures (indicated by TS) were located by using the Berny algorithm[16] until the Hessian matrix had only one imaginary eigenvalue. The identities of all transition states were confirmed by IRC calculations, and by animating the negative eigenvector coordinate with MOLDEN[17] and GaussView.[18]Approximate free energies (ΔG) and enthalpies (ΔH) were obtained through thermochemical analysis of frequency calculations by using the thermal correction to Gibbs free energy as reported by GAUSSIAN 03. This takes into account zero-point effects, thermal enthalpy corrections, and entropy. All energies reported in this paper, unless otherwise noted, are free energies or enthalpies at 298 K by using unscaled frequencies. All transition states are maxima on the electronic potential energy surface (PES), which may not correspond to maxima on the free energy surface. Calculations were performed for the gas phase with exception to the profile for **6a** and **6b**. Here polarizable continuum model (PCM) calculations[19] were also used to implicitly give an estimate for solvation effects. The solvent was dmso with ε = 46.826. *X*,*Y*,*Z* coordinates for all calculated compounds can be found in the Supporting Information.

Supporting Information (see footnote on the first page of this article): Computational details (coordinates and absolute energies), additional NMR spectra of all complexes, and the calculation of the reaction constants from the ^1H NMR spectra.

Acknowledgments

O. H. thanks Prof. Klaus Ruhland for helpful discussions.

[1] a) K. Öfele, *J. Organomet. Chem.* **1968**, *12*, 42–43; b) H.-W. Wanzlick, H. J. Schönherr, *Angew. Chem.* **1968**, *80*, 154–154; *Angew. Chem. Int. Ed. Engl.* **1968**, *7*, 141–142.

[2] A. J. Arduengo III, R. L. Harlow, M. Kline, *J. Am. Chem. Soc.* **1991**, *113*, 361–363.

[3] a) W. A. Herrmann, *Angew. Chem. Int. Ed.* **2002**, *41*, 1290–309; b) E. A. B. Kantchev, C. J. O′Brien, M. G. Organ, *Angew. Chem. Int. Ed.* **2007**, *46*, 2768–2813; c) S. Díez-González, S. P. Nolan, *Coord. Chem. Rev.* **2007**, *251*, 874–883.

[4] a) W. A. Herrmann, K. Öfele, M. Elison, F. E. Kühn, P. W. Roesky, *J. Organomet. Chem.* **1994**, *480*, C7–C9; b) K. R. Jain, W. A. Herrmann, F. E. Kühn, *Curr. Org. Chem.* **2008**, *12*, 1468–1478.

[5] a) H. Braband, T. I. Zahn, U. Abram, *Inorg. Chem.* **2003**, *42*, 6160–6162; b) T. I. Kückmann, U. Abram, *Inorg. Chem.* **2004**, *43*, 7608–7074; c) H. Braband, D. Przyrembel, U. Abram, *Z. Anorg. Allg. Chem.* **2006**, *632*, 779–785; d) H. Braband, E. Oehlke, U. Abram, *Z. Anorg. Allg. Chem.* **2006**, *632*, 1051–1056; e) E. Oehlke, T. Kückmann, U. Abram, *Z. Anorg. Allg. Chem.* **2007**, *633*, 830–834.

[6] C.-Y. Liu, D.-Y. Chen, G.-H. Lee, S.-M. Peng, S.-T. Liu, *Organometallics* **1996**, *15*, 1055–1061; a) W.-M. Xue, M. C.-W. Chan, Z.-M. Su, K.-K. Cheung, S.-T. Liu, C.-M. Che, *Organometallics* **1998**, *17*, 1622–1630.

[7] a) O. Kaufhold, A. Stasch, P. G. Edwards, F. E. Hahn, *Chem. Commun.* **2007**, 1822–1824; b) O. Kaufhold, A. Stasch, T. Pappe, A. Hepp, P. G. Edwards, P. D. Newman, F. E. Hahn, *J. Am. Chem. Soc.* **2009**, *131*, 306–312.

[8] a) W. A. Herrmann, D. Mihalios, K. Öfele, P. Kiprof, F. Belmedjahed, *Chem. Ber.* **1992**, *125*, 1795–1799; b) M. A. Huertos, J. Pérez, L. Riera, A. Menéndez-Velázquez, *J. Am. Chem. Soc.* **2008**, *130*, 13530–13531; c) O. Hiltner, E. Herdtweck, M. Drees, W. A. Herrmann, F. E. Kühn, *Eur. J. Inorg. Chem.* **2009**, *13*, 1825–1831.

[9] a) A. A. Gridnev, I. M. Mihaltseva, *Synth. Commun.* **1994**, *24*, 1547–1555; b) R. E. Cowley, R. P. Bontchev, E. N. Duesler, J. M. Smith, *Inorg. Chem.* **2006**, *45*, 9771–9779; c) J. Liu, J. Chen, J. Zha, Y. Zhao, L. Li, H. Zhang, *Synthesis* **2003**, *17*, 2661–2666.

[10] a) R. Alberto, R. Schibli, A. Egli, P. A. Schubiger, W. A. Herrmann, G. M. Artus, U. Abram, T. A. Kaden, *J. Organomet. Chem.* **1995**, *493*, 119–127; b) R. Alberto, A. Egli, U. Abram, K. Hegetschweiler, V. Gramlich, P. A. Schubiger, *J. Chem. Soc., Dalton Trans.* **1994**, 2815–2820.

[11] a) APEX suite of crystallographic software, *APEX 2*, version 2008.4, Bruker AXS, Inc., Madison, Wisconsin, USA, **2008**; b) *SAINT*, version 7.56a, and *SADABS*, version 2008/1, Bruker AXS, Inc., Madison, Wisconsin, USA, **2008**; c) A. Altomare, G. Cascarano, C. Giacovazzo, A. Guagliardi, M. C. Burla, G. Polidori, M. Camalli, *J. Appl. Crystallogr.* **1994**, *27*, 435–436; d) A. J. C. Wilson (Ed.), *International Tables for Crystallography*, Kluwer Academic Publishers, Dordrecht, The Netherlands, **1992**, vol. C, Tables 6.1.1.4 (p. 500–502), 4.2.6.8 (p. 219–222), and 4.2.4.2 (p. 193–199); e) G. M. Sheldrick, *SHELXL-97*, University of Göttingen, Göttingen, Germany, **1998** ; f) A. L. Spek, *PLATON, A Multipurpose Crystallographic Tool*, Utrecht University, Utrecht, The Netherlands, **2008**; g) *WinGX*, version 1.70.01 January 2005: L. J. Farrugia, *J. Appl. Crystallogr.* **1999**, *32*, 837–838; h) *POV-Ray*, version 3.6, **2004**, retrieved from http://www.povray.org/download/.

[12] M. J. Frisch, G. W. Trucks, H. B. Schlegel, G. E. Scuseria, M. A. Robb, J. R. Cheeseman, J. Montgomery, J. A., T. Vreven, K. N. Kudin, J. C. Burant, J. M. Millam, S. S. Iyengar, J. Tomasi, V. Barone, B. Mennucci, M. Cossi, G. Scalmani, N. Rega, G. A. Petersson, H. Nakatsuji, M. Hada, M. Ehara, K. Toyota, R. Fukuda, J. Hasegawa, M. Ishida, T. Nakajima, Y. Honda, O. Kitao, H. Nakai, M. Klene, X. Li, J. E. Knox, H. P. Hratchian, J. B. Cross, V. Bakken, C. Adamo, J. Jaramillo, R. Gomperts, R. E. Stratmann, O. Yazyev, A. J. Austin, R. Cammi, C. Pomelli, J. W. Ochterski, P. Y. Ayala, K. Morokuma, G. A. Voth, P. Salvador, J. J. Dannenberg, V. G. Zakrzewski, S. Dapprich, A. D. Daniels, M. C. Strain, O. Farkas, D. K. Malick, A. D. Rabuck, K. Raghavachari, J. B. Foresman, J. V. Ortiz, Q. Cui, A. G. Baboul, S. Clifford, J. Cioslowski, B. B. Stefanov, G. Liu, A. Liashenko, P. Piskorz, I. Komaromi, R. L. Martin, D. J. Fox, T. Keith, M. A. Al-Laham, C. Y. Peng, A. Nanayakkara, M. Challacombe, P. M. W. Gill, B. Johnson, W. Chen, M. W. Wong, C. Gonzalez, J. A. Pople, *Gaussian 03*, revision C.02, Gaussian, Inc., Wallingford, CT, **2004**.

[13] a) S. H. Vosko, L. Wilk, M. Nusair, *Can. J. Phys.* **1980**, *58*, 1200–1211; b) C. Lee, W. Yang, R. G. Parr, *Phys. Rev. B* **1988**, *37*, 785–789; c) A. D. Becke, *J. Chem. Phys.* **1993**, *98*, 5648–5652.

[14] a) W. J. Hehre, R. Ditchfield, J. A. Pople, *J. Chem. Phys.* **1972**, *56*, 2257–2261; b) M. M. Francl, W. J. Pietro, W. J. Hehre, J. S. Binkley, M. S. Gordon, D. J. DeFrees, J. A. Pople, *J. Chem. Phys.* **1982**, *77*, 3654–3665.

[15] a) P. J. Hay, W. R. Wadt, *J. Chem. Phys.* **1985**, *82*, 270–283; b) P. J. Hay, W. R. Wadt, *J. Chem. Phys.* **1985**, *82*, 299–310.

[16] H. B. Schlegel, *J. Comput. Chem.* **1982**, *3*, 214–218.

[17] G. Schaftenaar, J. H. Noordik, *J. Comput.-Aided Mol. Des.* **2000**, *14*, 123–134.

[18] R. Dennington II, T. Keith, J. Millam, K. Eppinnett, W. L. Hovell, R. Gilliland, *GaussView*, version 3.09, Semichem, Inc., Shawnee Mission, KS, **2003**.

[19] a) J. Tomasi, B. Mennucci, R. Cammi, *Chem. Rev.* **2005**, *105*, 2999–3093; b) M. Cossi, G. Scalmani, N. Rega, V. Barone, *J. Chem. Phys.* **2002**, *117*, 43–54; c) M. Cossi, N. Rega, G. Scalmani, V. Barone, *J. Chem. Phys.* **2001**, *114*, 5691–5701; d) V. Barone, M. Cossi, J. Tomasi, *J. Comput. Chem.* **1998**, *19*, 404–417.

[20] *WinDNMR: Dynamic NMR Spectra for Windows*: H. J. Reich, *J. Chem. Educ. Software*, 3D2, **1996**.

Received: June 24, 2010
Published Online: October 18, 2010

